ToF-SIMS Li Depth Profiling of Pure and Methylated Amorphous Silicon Electrodes After Their Partial Lithiation

Yue Feng, Bon Min Koo, Antoine Seyeux, Jolanta Światowska, Catherine Henry de Villeneuve, Michel Rosso, François Ozanam

ToF-SIMS Li Depth Profiling of *Pure* and *Methylated* Amorphous Silicon Electrodes after their Partial Lithiation

Yue Feng[a§], Bon-Min Koo[a§], Antoine Seyeux[b], Jolanta Światowska[b], Catherine Henry de Villeneuve[a], Michel Rosso[a], and François Ozanam[a*]

[a]Laboratoire de Physique de la Matière Condensée, CNRS, Ecole polytechnique, Institut Polytechnique de Paris, 91120 Palaiseau, France

[b]Chimie ParisTech - CNRS, PSL University, Institut de Recherche de Chimie Paris, 11 rue Pierre et Marie Curie, 75005 Paris, France

[*]E-mail: francois.ozanam@polytechnique.edu

[§]Y.F. and B.-M.K. contributed equally to this work

ABSTRACT: Pure (a-Si:H) and methylated (a-$Si_{0.95}(CH_3)_{0.05}$:H) amorphous silicon thin films were analyzed by time-of-flight secondary ion mass spectrometry (ToF-SIMS) after partial lithiation. Depth profiling gives insight into the lithiation mechanism of the material enabling to study the detailed biphasic process in the first lithiation process. Lithiation induces swelling and roughening of the active layer. In both a-Si:H and a-$Si_{0.95}(CH_3)_{0.05}$:H, no measurable Li diffusion was observed after stopping current-induced lithiation. After applying the same lithiation charges, distinct Li profiles were observed for these two materials. Unlike a-Si:H, the Li concentration drops slowly from the heavily lithiated region to the non-lithiated region in a-$Si_{0.95}(CH_3)_{0.05}$:H. This apparent progressive transition between the lithiated and lithium-free regions is attributed to the presence of nanovoids inside the material. When their concentration is high enough, these nanovoids constitute favorable quasi-percolating paths for lithium during the first lithiation. A specific model was developed to simulate the Li depth profiles, fully supporting this hypothesis.

KEYWORDS: *methylated amorphous silicon, lithium diffusion, ToF-SIMS, lithiation front, thin-film electrode, lithium-ion battery*

1. INTRODUCTION

In the last two decades, silicon has attracted a lot of interest for use as a high-capacity, low-potential anode material for advanced Li-ion batteries, opening new avenues for meeting the ever increasing demand for high-performance electrochemical energy storage devices.[1] The material still needs to overcome the two big challenges which prevent its application: mechanical fragility associated with massive lithium uptake and release, and poor surface chemical stability in the conditions of electrochemical cycling.[2-6] These drawbacks have limited the use of silicon in practical applications to Si incorporation in a small amount in composite electrodes[7]. Significant improvement in the performance of Si-based electrodes has been the design of composite electrodes with nano-sized Si particles, in order to better sustain the volume changes, and the engineering of sophisticated Si nanostructures, in order to benefit from chemically-stable interfaces.[8-10] Progresses in electrolyte formulation, binders, silicon surface treatments also achieve significant performance improvements.[11-14] Nevertheless, none of these advances up to now demonstrates a true capability of upscaling to commercial achievement.

In this context, a clear understanding of processes which take place during the lithiation and delithiation of the material appears instrumental for opening new perspectives.[15-17] We contribute to this effort by studying in details a new class of materials, methylated amorphous silicon,[18] derived from the well-known hydrogenated amorphous silicon (a-Si:H, hereafter abbreviated as a-Si). In the context of Li-ion batteries, these materials have shown a significantly better tolerance to lithiation/delithiation cycles as compared to amorphous silicon.[19] It has been shown that the material undergoes a first electrochemical lithiation according to a biphasic process,[20] like crystalline[21, 22] or amorphous[23, 24] silicon.

ToF-SIMS is a surface-sensitive technique that allows for the detection of trace elements. When associated to layer etching, it provides elemental and molecular profiles as a function of depth (a few angstroms to hundreds of nanometers), which offers an attractive opportunity for

determining Li profiles in electrochemically lithiated Si electrodes.[25-27] Using ToF-SIMS, we have already demonstrated in-depth characterization of the chemical and morphological modifications during lithiation/delithiation of a-Si thin films deposited by PECVD.[26] Using a similar approach, the investigation of the lithiation mechanism of methylated amorphous silicon (methylated a-Si) with different methyl-group concentrations is of great interest, since the first lithiation in methylated amorphous silicon has been proved to present distinct features from that of a-Si.[28, 29] We present here a ToF-SIMS study aiming at determining the depth profile of Li during the first lithiation of methylated a-Si, using an experimental approach allowing for achieving an improved depth resolution. Questions of special interest are about the direct confirmation of the biphasic character of the first lithiation of methylated a-Si, and a possible relaxation of Li concentration by diffusion after the release of the electrochemical control.

2. EXPERIMENTAL PROCEDURES

2.1 Preparation of partially lithiated amorphous silicon electrodes.

100 nm-thick pure a-Si and 5% methylated a-Si layers were deposited by plasma enhanced chemical vapor deposition (PECVD) at 250°C[18, 30] on a crystalline silicon substrate (15 × 15 mm^2, 500 µm thick). Here, the use of a silicon substrate has been preferred to a metallic substrate, the usual choice in ToF-SIMS investigations on thin active-material layers in the battery context.[25-27] As it will be explained in section 3, the interest of this substrate is to have a very flat surface, allowing for an accurate measurement of the concentration profiles. The crystalline Si substrates (denoted c-Si in the following) were cut from n-type, (100) oriented, one-side polished, float-zone purified silicon wafers (Siltronix France), with 1-100 Ω cm resistivity. The precursor gas was silane or a silane/methane mixture. The following parameters were set during deposition: plasma excitation frequency of 13.56 MHz; excitation power of 0.10 W cm^{-2}; pressure of 0.5 mbar.[18] In this condition, SiH_4 molecules are directly decomposed,

but not CH_4. Therefore, when present, carbon is incorporated into the amorphous silicon layer under the form of methyl groups only.

The lithiation of the Si layers was performed in a homemade two-electrode half cell as shown in **Figure S1**. The assembly of the cell and the lithiation were carried out in a glove box under argon atmosphere (O_2 < 10 ppm, H_2O < 5 ppm). The working electrode and counter electrode were, respectively, the methylated or pure a-Si layer and a Li-metal sheet (99.9% purity, Aldrich). 1 M $LiClO_4$ (battery grade, 99.99% purity, Aldrich) in propylene carbonate (PC) (99.7% purity, Sigma-Aldrich) was used as the electrolyte. The electrodes were lithiated galvanostatically using an Autolab PGSTAT12 at room temperature (20-23 ˚C). The active area for lithiation was 0.79 cm^2, as defined by the inner diameter of the O-ring in the electrochemical cell. a-Si was lithiated at 20 μA (25.32 μA cm^{-2}, at a rate around C/3, i.e., full lithiation in 3 hours) for 30 min. The first lithiation is homogeneous at this current density, i.e., lithiation proceeds at the same rate at each location over the surface. This behavior has been confirmed by in situ optical microscopy (**Figure S2a**). However, in the same electrochemical conditions, the first lithiation of 5% methylated a-Si is inhomogeneous, i.e., it initiates at some spots over the surface of the electrode which then radially expands. This inhomogeneity arises from the high resistivity of methylated a-Si.[29] As a matter of fact, the a-Si resistivity is of the order of 10^8 Ω cm, and that of 5% methylated a-Si is ~10^{10} Ω cm, as determined by current-voltage measurements in the space-charge-limited-current (SCLC) regime in a sandwich geometry.[31, 32] To get a homogenous first lithiation, 5% methylated a-Si electrode was lithiated at a smaller current: 1 μA (1.27 μA cm^{-2}, around C/60) for 10 h (see **Figure S2** in supplementary information for further details concerning the effect of current density on the homogeneity of the first lithiation of 5% methylated a-Si electrodes).

After lithiation, the Si layers were rinsed first with propylene carbonate (PC) to remove residual lithium salts, and then with highly volatile dimethyl carbonate (DMC) to remove the

PC remaining on the Si surface. All these cleaning treatments were done in the glove box. After rinsing, the samples were put in a tightly-closed transfer case under an argon atmosphere, and then transferred to another glove box (O_2 = 7 ppm, H_2O = 0.6 ppm) coupled to the ToF-SIMS spectrometer.

2.2 ToF-SIMS. ToF-SIMS measurements were conducted with an IONTOF ToF-SIMS 5 spectrometer. The dual beam analysis mode in the High Current Bunched mode (HC-Bunched) was used to get in-depth profiles with a high mass resolution (M/ΔM=8000). A pulsed 25 keV Bi^+ (pulse duration of 60 μs) delivering 1 pA current over a 100 × 100 μm^2 area was used for analyzing the surface, and a 2 keV Cs^+ beam delivering 80 nA over a 300 × 300 μm^2 area was used for sputtering. At each sputtering step, the analysis was performed at the center of the sputtered crater to avoid edge effect. Both ion beams have an incident angle of 45° on the sample surface. A crucial point for the acquisition of relevant ToF-SIMS profiles is to probe samples which are homogeneous at the scale of the analyzed zones, as shown in **Figure S3**. This requirement motivates the choice of the lithiation conditions described in the previous section. The main chamber pressure was maintained in a ultra high vacuum (UHV) range at 10^{-9} mbar. Data acquisition and processing were performed using the IonSpec commercial software.

The pure a-Si electrode has been characterized at various times after stopping its lithiation: 43 min, 1h 35 min, 2 h 35 min, 4 h 35 min, 21 h 33 min. For 5% methylated a-Si, the times elapsed after stopping lithiation are: 51 min, 1h 30 min, 2 h, 3 h, 4 h, 5 h, 6 h, 7 h, 8 h, 9 h, 10h. The minimum time (43 and 51 min) corresponds to the typical time needed for the transfer procedure of the lithiated electrodes to the ToF-SIMS spectrometer and the acquisition of the first ToF-SIMS profile.

All the depth profiles were recorded in negative polarity. The ion selected for depth profiling were Si_2^- and SiO_2^- (characteristic species for silicon and silicon oxide, respectively),

SiH^- (characteristic of the hydrogenated nature of the deposited Si), SiC^- (characteristic of methylated a-Si), and Li^-, Cl^- and CO_2^- (characteristic of Li, chloride and carbonate species, respectively).

3. RESULTS AND DISCUSSION

3.1 Non-lithiated samples.

3.1.1 Influence of the electrode substrate on the depth profile resolution.

ToF-SIMS profiles of SiH^- and SiO_2^- ions measured in pristine a-Si samples deposited either on a crystalline silicon substrate (c-Si, red lines) or a stainless steel substrate (SS, black lines) are compared in **Figure 1**. On the SiH^- profiles (**Figure 1a)** two regions are clearly distinguished: one region corresponding to the hydrogenated a-Si layer (high SiH^- intensity, grey area), and the other to the substrate (lower SiH^- intensity, sputtering time > 210 s). On the SiO_2^- profiles the a-Si layer / substrate interface is outlined by the presence of peaks indicating a surface oxidation of the substrate. On the SiH^- profile, the peak at the interface of the electrode with the c-Si substrate is also related to the substrate oxidation.[33, 34] Such an *"artificial"* enhancement of ToF SIMS signals is associated to a local chemical composition change of the analysed solid. This phenomenon is well known and is generally described as matrix effects.[35, 36]

Strikingly, a broader transition is observed at the a-Si layer / SS substrate interface for the two types of ionic species (**Figure 1**, blue lines). In both cases (SiH^- and SiO_2^- profiles), the apparent interface widths correspond to ~50% of the a-Si layer thickness which limits the accuracy of the depth analysis in the film. Such broad interfaces originate from a surface roughness effect. Conversely, much sharper transitions are observed in the case of the a-Si layer deposited on the c-Si substrate (**Figure 1**, red lines). The use of flat substrates – as crystalline

silicon – makes clear that the intrinsic depth resolution of the technique (limited, e.g., by the uniformity of the etching) is ~2 nm (determined from the full width at half maximum –FWHM– of the interface peak on the SiH^- profile on a linear scale), as deduced from the thickness (100 nm) of the as-deposited a-Si layer. In the context of the investigation of the lithiation of (methylated) a-Si layers, it could be questioned whether using a silicon substrate could introduce artifacts, such as the lithiation of the substrate. Actually, as far as the potential is kept above 0.1 V *vs.* Li/Li^+ lithiation of c-Si is not expected: as it will appear below, no lithium is detected in the substrate in the experiments reported hereafter.

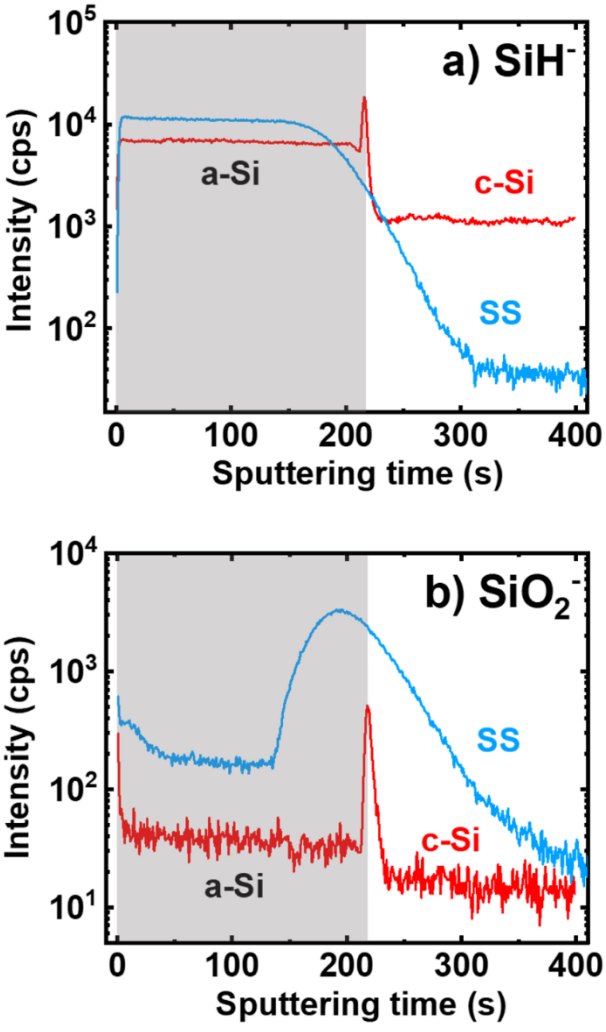

Figure 1. ToF-SIMS profiles of SiH^- (a) and SiO_2^- (b) ions for a 100 nm–thick a-Si layer deposited on a stainless-steel (SS) (in blue) and crystalline Si (in red) substrate. The interface

between the layer and the substrate appears much broader on the SS substrate than on c-Si, showing the interest of using a very flat substrate.

3.1.2 Composition of pristine a-Si and 5% methylated a–Si electrodes.

The concentration profiles of some ionic species for a pristine a-Si and 5% methylated a-Si electrodes are shown in **Figure 2**. The set of ion profiles has been chosen for giving the most representative picture of the composition of the layers.

SiH^- and SiC^- ions are species characteristic of the deposited layers, allowing for distinguishing in the profiles the region corresponding to the deposited layer (highlighted in red in **Figure 2**), and that corresponding to the substrate (highlighted in blue in **Figure 2**). SiH^- species are detected in the bulk of both layers at levels much larger than in the substrate, confirming the hydrogenated nature of both materials. In contrast and as expected, a significant intensity of SiC^- ions is found in the methylated material only. The composition of the layers appears quite homogeneous in depth, since SiH^- and SiC^- profiles are constant over the full layer thickness. In particular, the flat profile of SiC^- ions indicates that, at the z-resolution of the ToF-SIMS analysis, the distribution of methyl groups is homogeneous in depth in the methylated a-Si layer.

Significant amounts of oxygenated species (SiO_2^-) are found at the buried interface and at the external surface indicating a surface oxidation of the substrate and the a-Si layers respectively. The presence of a local variation of the composition (surface oxidation) at the a-Si electrode surface and at the buried interface induces changes in the ionization yields for other non-oxygenated ionic species (matrix effects), leading to an "artificial" raising of their intensity (peaks observed at the outer surface or at the buried interface).

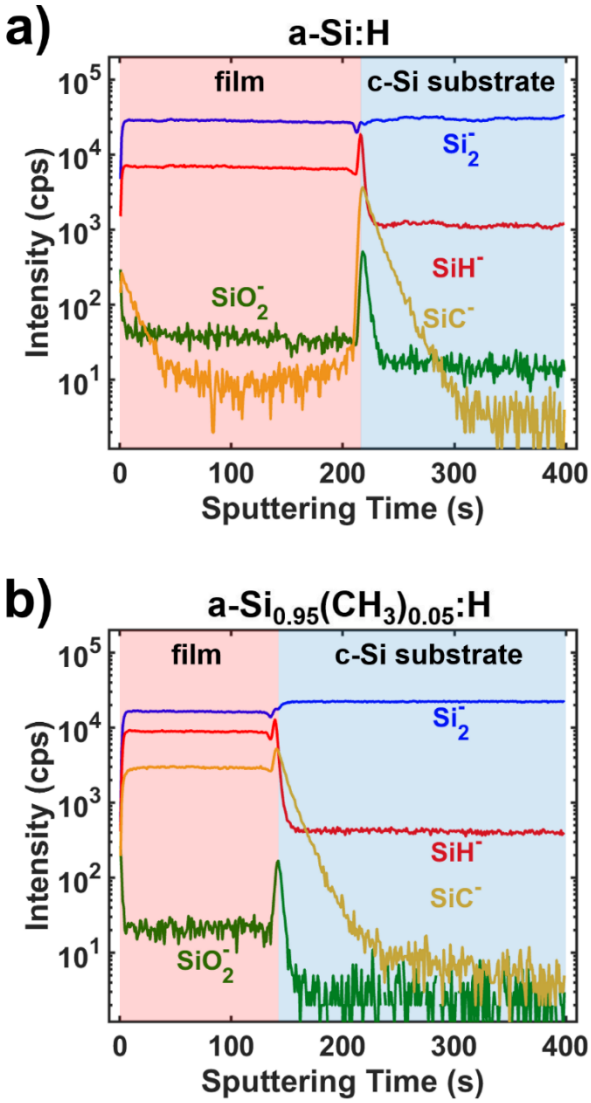

Figure 2. ToF-SIMS profiles (Si_2^-, SiH^-, SiC^-, and SiO_2^-) for 100 nm–thick films of a-Si (a) and 5% methylated a-Si (b) deposited on crystalline-Si substrates.

3.2 Partially lithiated samples.

a-Si and methylated a-Si electrodes have been partially lithiated up to ~ 10 µA h, as described in Section 2.1. Full lithiation of the thin-film electrodes corresponds to a charge of ~ 60 µA h. The value of 10 µA h has been chosen in order to remain to the first half of the potential plateau corresponding to the biphasic regime of the first lithiation for pure and 5% methylated a-Si.[Ref 20, Koo et al.] The evolution of the electrode potential during the lithiation are shown **in Figure**

S4. ToF-SIMS profiles (raw data) of various ionic species measured after the lithiation are shown in **Figure 3** (solid lines).

The SiH^- profile obtained for the partially lithiated a-Si electrode is compared to that corresponding to a pristine electrode (**Figure 3a**, dashed red line). A first conspicuous observation is that the etching time needed to fully etch the lithiated layer and reach the substrate (275 s) is significantly larger than the one needed to etch the non-lithiated material (220 s). A similar effect is observed for the methylated material. In this case the layer / substrate interface is reached at 175 s (**Figure 3b**) instead of 140 s for the pristine electrode (**Figure2b**). The observation of the buried interface for larger etching times is consistent with an increase of the active layer thickness (swelling) induced by lithium incorportion (a moderate swelling due to partial lithiation). A similar observation was already reported previously. [26] Moreover, it can be noticed that the width of the SiH^- peak at the layer/substrate interface is significantly broader in the case of the lithiated electrode (FWHM ~15 s, corresponding to a depth of ~7 nm, whereas the FWHM is ~4 s for the pristine electrode). The observation of the peak broadening indicates that the lithiation-induced swelling of the layer leads to a significant roughening of the external surface of the electrode. Since the layer is expected to etch at a constant rate with no significant planarization upon etching, a surface roughening induces broader interface transitions associated to ionic concentration changes all along the sputtering depth.[26]

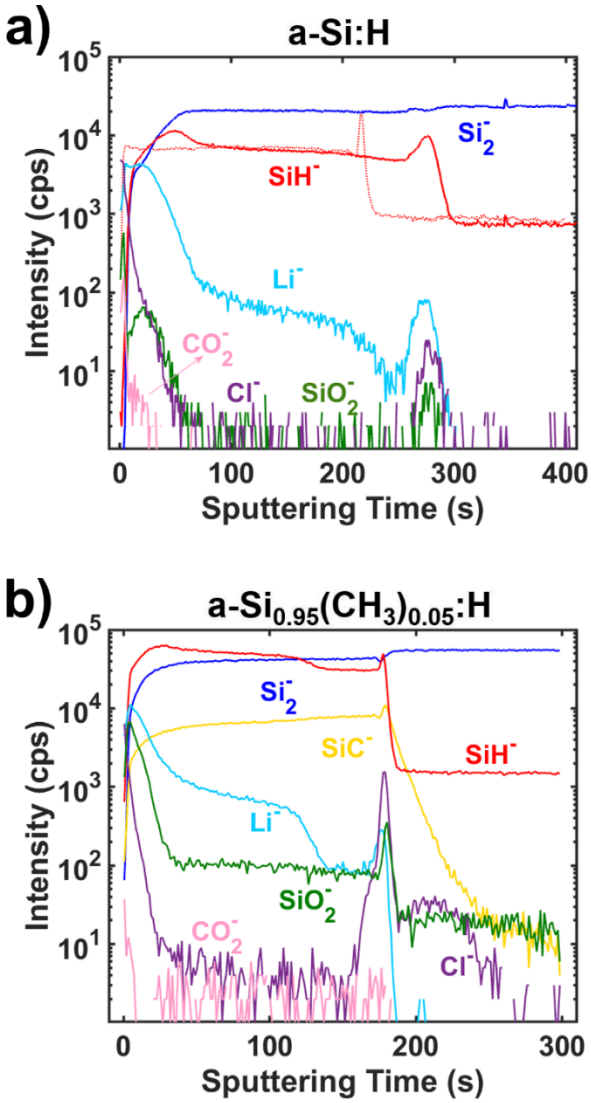

Figure 3. ToF-SIMS profiles after partial lithiation of a-Si at a lithiation rate of ~C/3 (a) and 5% methylated a-Si at a lithiation rate of ~C/60 (b). In a), the SiH^- profile recorded on a non-lithiated layer (dashed lines) is also plotted for comparison.

For both electrodes, some ions characteristic of electrolyte species or products of electrolyte decomposition (Cl^-, CO_2^-) exhibit a maximum at very short sputtering times, corresponding to a region at the outermost surface (interface with the electrolyte) of the lithiated material. As expected, they reveal the formation of a thin SEI layer during the first part of the lithiation, in agreement with previous reports.[14, 25] The significant decrease of the signal corresponding to these ionic species after a few seconds of sputtering time allows for

positioning the SEI / electrode interface. Beyond this time, the ionic species detected can be assigned to the lithiated layer.

The Li^- ion profile deserves special attention and will be addressed in Section 3.3 and 3.4.

3.3 Time evolution of the Li profile.

The ion profiles presented in **Figure 3** are raw data recorded right after the introduction of the electrodes in the UHV measurement chamber. These first measurements were carried out 43 min (pure a-Si) and 51 min (5% methylated a-Si) after the interruption of the lithiation. In order to assess a possible evolution of the Li^- distribution upon time (e.g., through diffusion), the samples have been kept for a few hours in the UHV chamber and profiles have been recorded at various times after the end of the lithiation. The raw Li^- profiles and those obtained after data processing allowing for their comparison are displayed in **Figure 4**.

Figure 4a displays the raw experimental profiles recorded for pure a-Si and 5% methylated a-Si electrodes after various waiting times. Their careful comparison requires : i) the adjustment of the offset of the time scale (which might vary, e.g., upon possible local variations of the SEI thickness), ii) the adjustment of the time-to-thickness conversion factor (which might slightly vary due to minute changes in the experimental etching rates on a few-hour timescale) and iii) the normalization of the signal (whose magnitude might also vary due to minute variations of the primary-ion beam intensity on the same timescale).

The signal from Cl^- ions has been used for correcting the offset of the time scales. The origin of the time scale has arbitrarily been fixed at the time where the Cl^- profile has decreased by a factor of two from its maximum value (located at the first point of the profile in most of the cases). The time-corrected profiles are shown in **Figure 4b**. The time corrections span between 4 and 9 s for the corresponding data recorded for pure a-Si, and between 2 and 3 s for 5% methylated a-Si in **Figure 4b**.

The need for correcting the time-to-thickness factor clearly appears on **Figure 4b** in view of the variable positions of the peak related to the buried active layer/substrate interface. This position indicates the time needed for a complete etching of the layer (which is 100 nm thick in its pristine state, but thicker in its partially lithiated state). The profiles have then been replotted as a function of a normalized depth, by applying a linear transformation of the time scale aiming at setting the peak position to 1. The corresponding plots are drawn in **Figure 4c**. The correction factors span between 0.0035-0.0037 for pure a-Si, and between 0.0053-0.0059 for 5% methylated a-Si.

The convenient comparison of the profiles also calls for adjusting the signal amplitudes through a relevant normalization procedure. For that purpose, the Li^- counts have been divided by a value corresponding to the average count of the Si_3^- ions measured in the substrate (normalized depth from 1.1 to 1.5). The resulting profiles are plotted in **Figure 4d**. As it immediately appears, for both electrodes, all the profiles recorded at various times after lithiation (up to 20 hours for a-Si electrode and 10h for methylated electrode) nearly perfectly coincide. If Li diffusion would take place from the region of high lithium content to the region of low lithium content, the Li concentration in the region of low lithium concentration should exhibit a complementary error function profile with a characteristic length equal to $(4Dt)^{1/2}$, where D is the diffusion coefficient and t the elapsed time after the end of lithiation. Even with the lowest values reported for D, on the order of a few 10^{-15} cm^2 s^{-1},[37] a characteristic diffusion length on the order of 250 nm would be expected after 10h, which is much larger than the thickness of the active layer. It then appears that the distribution in the partially lithiated materials is frozen: no lithium motion can be evidenced over several hours under UHV after the interruption of the electrochemical lithiation, despite the inhomogeneous distribution of Li within the thin active layer. This is significantly different than for the amorphous high-lithium-content region, where, relatively fast Li dynamics have been measured using Nuclear Magnetic

Resonance, with room-temperature diffusion coefficients on the order of 10^{-9} cm^2 s^{-1}. [Dunst, A.; Sternad, M.; Epp, V.; Wilkening, M., Fast Li+ Self-Diffusion in Amorphous Li−Si Electrochemically Prepared from Semiconductor Grade, Monocrystalline Silicon: Insights from Spin-Locking Nuclear Magnetic Relaxometry, *Journal of Physical Chemistry C*, **2015**, 119, 12183-12192.] The same trends (faster diffusivity of Li in Li-Si compounds) are obtained from tracer-diffusion experiments on sputtered amorphous Li-Si layers [Strauß, F.; Hüger, E.; Julin, J.; Munnik, F.; Schmidt, H., Lithium Diffusion in Ion-Beam Sputter-Deposited Lithium−Silicon Layers, *Journal of Physical Chemistry C*, **2018**, 122, 8616-8623.] It should also be noted that the shape of the profile recorded in pure a-Si is compatible with a single-step biphasic mechanism, in contrast to the two-step biphasic process observed in sputtered amorphous silicon. In the later case, ToF-SIMS investigations have shown that lithiation occurs first through a biphasic lithiation with an invading phase of relatively low Li content (Li:Si ~ 3:10), then through a second biphasic process where the invading phase had a much higher Li content. [Hüger, E.; Jerliu, B.; Dörrer, L.; Bruns, M.; Borchardt, G.; Schmidt, H., A Secondary Ion Mass Spectrometry Study on the Mechanisms of Amorphous Silicon Electrode Lithiation in Li-Ion Batteries, *Zeitschrift für Physikalische Chemie*, **2015**; 229, 1375–1385. Uxa, D.; Jerliu, B.; Hüger, E.; Dörrer, L.; Horisberger, M.; Stahn, J.; Schmidt, H., On the Lithiation Mechanism of Amorphous Silicon Electrodes in Li-Ion Batteries, *Journal of Physical Chemistry C*, **2019**, 123, 22027-22039.] As suggested by the authors, this two-step process likely arises from a first facile lithiation of the numerous defects and dangling bonds present in sputtered amorphous Si. These defects are mostly cleared out in hydrogenated a-Si grown by PECVD, consistently accounting for a single-step biphasic process in the present study.

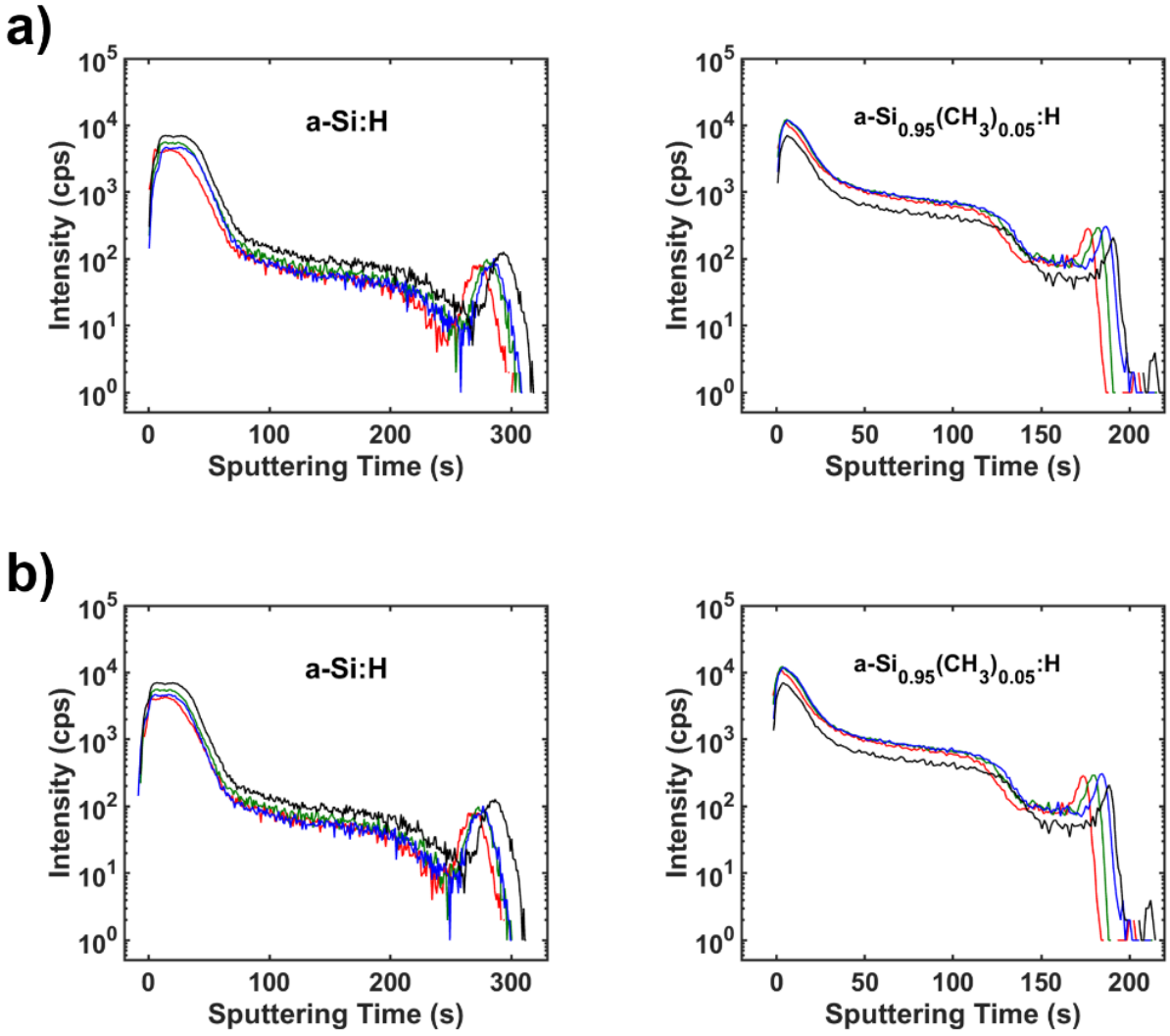
a)
a-Si:H
a-Si0.95(CH3)0.05:H
Intensity (cps)
Sputtering Time (s)
b)
a-Si:H
a-Si0.95(CH3)0.05:H
Intensity (cps)
Sputtering Time (s)

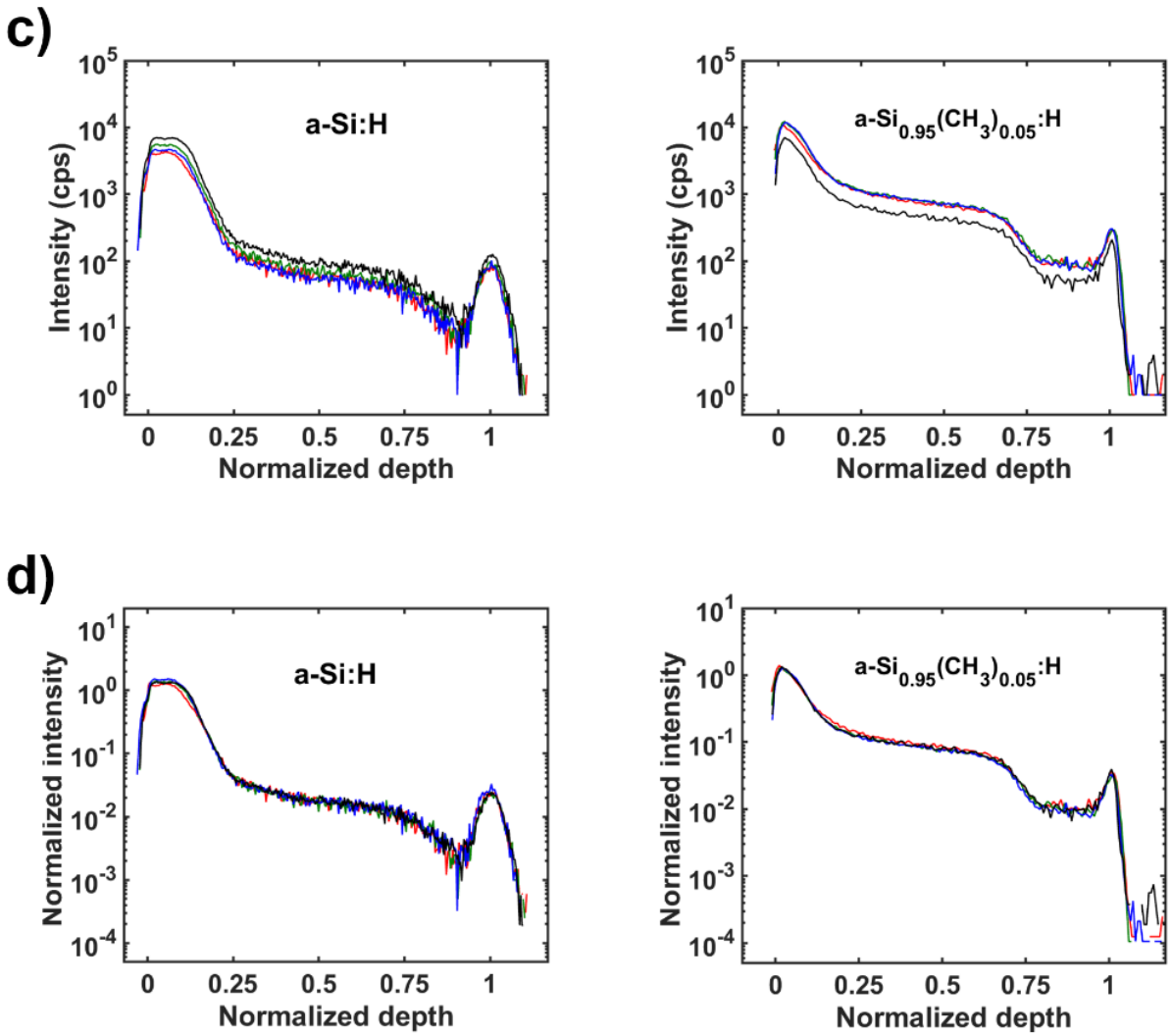

Figure 4. Comparison of Li^- profiles for increasing waiting times after lithiation for a-Si (left column) and 5% methylated a-Si (right column). The times elapsed after lithiation are 43 min (red line), 2h35 (green line), 4h35 min (blue line) and 21h33 min (black line) for a-Si, and 51 min (red line), 4h (green line), 7h (blue line) and 10h (black line) for 5% methylated a-Si. (a) Raw Li^- profiles. (b) Profiles after adjusting the SEI/active layer interface at time 0. (c) Same as in (b) after conversion of time into normalized depth (see text). (d) Same as in (c) after intensity normalization to the intensity of the Si_3^- signal in the substrate.

3.4 Comparison of Li distribution in methylated and non-methylated electrodes.

For quantitative comparison, the Li profiles obtained for a-Si (blue) and methylated a-Si (red) are plotted using a linear vertical scale in **Figure 5**. The profiles correspond to the first ones measured after lithiation and were corrected according to the procedure described in section 3.3. The colored/hashed part of the plots represent 95% of the incorporated Li. Several regions corresponding to different Li contents are distinguished within the active layers. In the case of the *non-methylated* material, Li is mainly present in the subsurface region and only at trace level deeper in the bulk of the electrode. In the case of the *methylated* electrodes, a Li-rich region is also observed nearby the surface, but narrower than for the non-methylated material. In this case, the Li content within this Li-rich subsurface region corresponds to only ~ 50% of the total Li amount. Remarkably, in contrast to the non-methylated electrode, a non negligible Li content is detected deeper in the core of the electrode (intermediate [Li] region in **Figure 5b**).

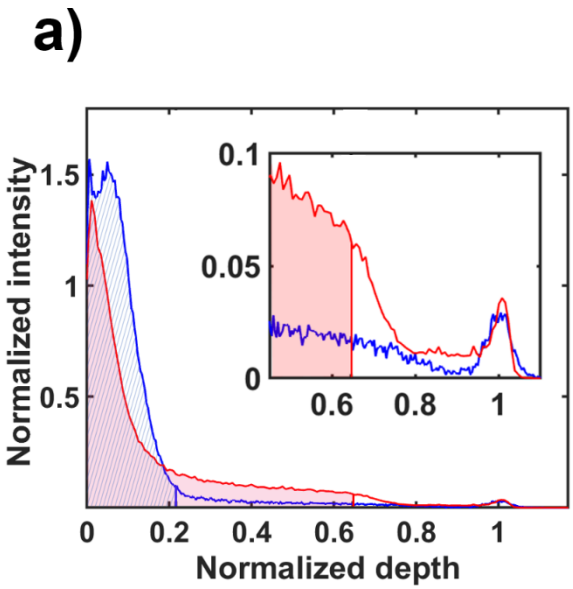

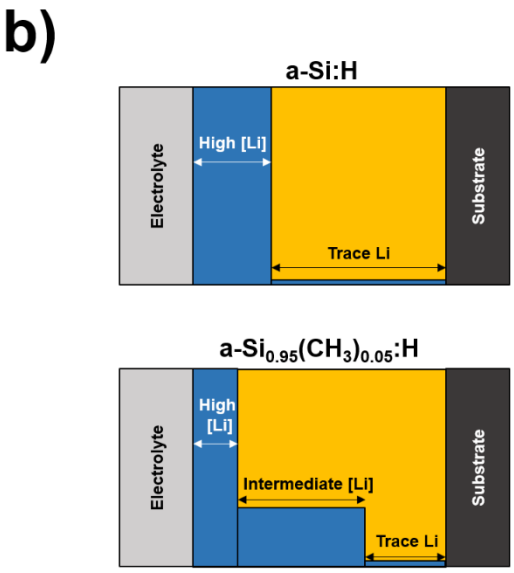

Figure 5. (a) Li^- profiles as a function of depth for partially lithiated a-Si (blue line) and methylated a-Si electrodes (red line). The profiles (recorded 43 min and 51 min, respectively, after the end of lithiation) are the same as those shown in **Figure 4d**, here plotted in linear scale. The colored and hashed areas correspond to 95% of the Li incorporated inside the electrode. The inset shows the profiles in the 0.45-1.1 depth range at an enlarged vertical scale. (b) Sketch of the Li repartition in a-Si and 5% methylated a-Si. Two regions of high concentration and trace amount of Li are present in a-Si, and a third one of intermediate Li concentration is also present in 5% methylated a-Si.

Several issues should be considered to afford a reliable comparison of the Li profiles in pure and methylated a-Si electrodes. From a quantitative point of view, when comparing the profiles in **Figure 5a**, it is noticed that the integral of the two profiles is nearly the same. It is tempting to turn Li^- counts in terms of Li concentration; then, the similarity of the profile integrals could be paralleled with the nearly equal electrochemical charge used for lithitation. However, this comparison cannot be made accurately. First, matrix effects may need to be considered. Specifically, the presence of a strong increase of the lithium profile close to the surface could

be questioned. Oxide is present at the SEI/layer interface as well as at the layer/substrate one, as revealed by the SiO_2^- profile. The presence of oxygen is known to significantly enhance the ionization yield of negative ions. Even if such an effect may change the magnitude of the detected signals, it does not appear to significantly affect the general shape and behavior of the profile, especially the presence of a high-Li-concentration region close to the surface. In pure a-Si and methylated a-Si, the SiO_2^- signal also exhibits a peak close to the interface with SEI, but the signal values remain weak, especially in the case of pure a-Si (**Figure 3**). Thus, if oxygen-induced matrix effects would be responsible for the appearance of a peak in the Li profile close to the surface, such a peak would be much less marked in the case of pure a-Si than for 5% methylated a-Si. This is not the case. Therefore, though the magnitude of matrix effects has not been precisely assessed, they appear weak enough for warranting the actual existence of a heavily lithiated region close to the surface in partially lithiated pure a-Si and, plausibly, in 5% methylated a-Si. On the other hand matrix effects might well explain the presence of the increase of the lithium profile close to the layer/substrate interface.

The correction procedure explained in section 3.3 overlooks a quantitative difference between the two Li^- profiles shown in **Figure 5** even though the scaling performed on the time scale should correct the differences in the etching rate of the materials in the two experiments. The layer thickness is expected to be somewhat different in the two experiments, since the concentration in Li^- of the invading lithiated phase is expected to be lower for 5% methylated a-Si than for pure a-Si.[20] The lower Li concentration after partial lithiation of 5% methylated a-Si should lead to lower swelling (thinner layer) than for pure a-Si. Therefore, it seems challenging to accurately compare the two profiles, and we will mainly discuss the shape and the order of magnitude of the Li intensity profiles. In the following, the ToF-SIMS ion profiles will be discussed in terms of changes in Li concentration in the solid phase, though such an

identification is strictly speaking abusive. It mainly relies on the above remark that matrix effects remain weak.

It has already been mentioned that the first lithiation of Si,[21, 22, 38, 39] a-Si,[23, 24] and methylated a-Si[20] proceeds according to a biphasic mechanism. Therefore, the existence of a near-surface region in which the lithium concentration is high is an expected feature for both pure a-Si and 5% methylated a-Si. Nevertheless, this simple scheme does not account for the non-null Li concentration observed beyond the high Li-concentration region both for pure a-Si and for 5% methylated a-Si. In the latter case however, the Li- count is much higher than in pure a-Si and the low-concentration region seems to split into two sub-regions (see **Figure 5b**, intermediate and trace regions): this will be discussed in a second stage.

We first discuss the presence of a small amount of Li present in the bulk of the partially lithiated electrodes (trace Li region in **Figure 5b**) or at the interface with the substrate. On general grounds, the tailing of the concentration of atoms present at the surface or near the surface deeper in the profiling of a thin layer can arise from a mixing effect generated by the atomic collision cascade triggered by the primary ion beam. It is the well-known "knock-in" effect whose magnitude is known to be large for light atoms and light and energetic ions.[40] The induced tailing can typically extend over several tens of nanometers and account for the Li traces extending up to 80% of the depth of the thin layer of pure a-Si (see **Figure 5a**). Besides this effect, other possibilities might be invoked for accounting for the existence of a non-null lithium concentration extending far away from the heavily lithiated phase close to the surface. For instance, neutron reflectivity experiments have reported the existence of deep lithiation in crystalline Si at a Li concentration lower than that found close to the surface (typically by a factor of 25).[41] However, these operando measurements have been performed in very specific electrochemical conditions, which restrict the first lithiation (even "deep lithiation") at depths below 50 nm, in marked contrast with what is observed in our experimental conditions.

Therefore, it appears difficult to compare the results obtained by neutron reflectivity to the present results.

Other results obtained by ToF-SIMS on PVD-deposited amorphous silicon thin films have been obtained in conditions more comparable to ours.[27] Deep lithiation at a Li concentration lower than that close to the surface has also been reported. This phenomenon has been ascribed to the presence of defects leading to the diffusion of Li throughout the Si layer. Such defects are often found in PVD coatings. An accumulation of Li at the back interface was also mentioned in support of this attribution. In the present study, the material has been grown using PECVD and not deposited using PVD. However, pinholes are well-known defects in PECVD-grown a-Si films.[42] The existence of depressions in the layer (local low-thickness defects) of micrometric lateral extension and a few 10-nm depth has directly been evidenced by confocal microscopy on our methylated a-Si layers.[29] As mentioned above, the Li peak detected at the back interface (see **Figure 4d**) can at least be in part associated to matrix effects linked to the presence of Si oxide at this interface. Therefore, although a Li accumulation at the back surface cannot be excluded, the present results do not give a clear indication of its existence. However, defects in the deposited layer might possibly contribute to the presence of lithium in the region deeper than the interface between the heavily lithiated phase and the non-lithiated part. No detailed investigations have been tried to determine the origin of this region of low but finite Li content in pure a-Si.

We rather focus on the case of 5% methylated a-Si for which two sub-regions of finite and distinct lithium concentration exist, with a region of intermediate Li concentration between the heavily lithiated region and the region of lower Li content where the presence of lithium can be ascribed either to depression-like defects or mixing effects during profiling. This region of intermediate Li concentration appears specific to the experiments performed on 5% methylated a-Si. One could then question the influence of the lithiation charging rate, since it

has been found necessary to lithiate 5% methylated a-Si at a much slower rate than pure a-Si to ensure the lithiation spatial homogeneity. However, this origin appears unlikely. Low charging rates make less stringent the limitations associated with kinetics and low-mobility species in the solid phase during lithiation. One could then argue that the intermediate Li concentration region arises from Li diffusion from the heavily lithiated face toward the back interface. But this explanation seems to be inconsistent with the frozen character of the Li distribution on a several-hour timescale after the interruption of the lithiation (**Figure 4d**). Therefore, diffusion does not seem to be involved. Apart from diffusion, the other consequences of a low charge rate would favor the uniformity of the lithiation (like the case regarding the lateral homogeneity) rather than spreading or inhomogeneity of the lithiation. The existence of the region of intermediate Li concentration might then be accounted for by the inhomogeneity of methylated a-Si at the nanometric scale. The presence of nanovoids in the material microstructure has already been suggested to account for the variation of the stoichiometric content of the heavily lithiated phase as a function of the methyl content of the material in previous studies.[20] It has also received indirect experimental support from SAXS measurements.[43] These nanovoids are thought to arise from the need to locally adapt the atomic Si arrangement to the bulky methyl groups while keeping the tetrahedral bonding configuration of Si atoms as less distorted as possible. These nanovoids are thought to provide easy lithiation sites on their internal walls,[20] thus creating faster lithiation paths in the material by minimizing the amount of hard material to be disrupted for going from one nanovoid to another neighboring one.

A specific model has been worked out and simulated in order to test the effect of such a general mechanism. This model assumes that lithiation occurs from the surface in contact with the electrolyte by a progressive invasion of a lithiated phase. Nanovoids are present in the layer with a given size and a given volume distribution. It is assumed that when the lithiation front reaches a nanovoid, the entire volume associated with the nanovoid is immediately filled with

lithium, providing an instantaneous progression of the lithiation front in the considered nanovoid. Otherwise, the lithiation front progresses nearly uniformly at the other locations not in contact with a nanovoid, as schematized in **Figure 6a**. More precisely, the local progression of the front is modulated in order to account for the disordered nature of the material. The model is designed to capture the main feature to be tested: the involvement of nanovoids in creating preferred lithiation paths. It is not aimed at capturing the whole physico-chemical processes at work in the lithiation (e.g., no explicit consideration is made to account for the lithiation-induced stresses that are thought to assist the progression of the lithiation front).

Specifically, the model is implemented in a simulation performed on a x=120, y=120, z=140 cubic lattice. According to the material density,[43] in 5% methylated amorphous silicon 10% of the lattice sites are empty. They are considered as voids and are randomly distributed in the 3D grid. All lattice sites are occupied in the case of pure a-Si. In the initial time step of the simulation, it is assumed that all sites on the basal surface (which features the surface in contact with the electrolyte) define the departure of the lithiation front. The electrolyte/electrode interface is at z=0, the lithiation proceeds along the z axis. The calculation represents a charge at constant current: at each time step of the calculation, a constant number of Li (n_{Li}) are inserted in the lattice (500 in the actual calculation). In order to account for the easy lithiation of voids, priority is given to empty sites. Then if n_v (number of voids) empty sites have been lithiated at a time step, $500–n_v$ occupied sites are lithiated. An empty site can be lithiated if a neighboring site is lithiated. Among the numerous occupied sites that can be lithiated (because they are neighboring lithiated sites) the sites with the maximum number of lithiated neighbors at lower z are lithiated. Therefore, for a given distribution of the voids, the evolution of the lithiation is deterministic.

In the absence of voids, a flat lithiation front progressively moves from the basal plane to the top plane, a good description of a usual biphasic lithiation process. The Li concentration

as a function of z is calculated at different time steps. The result of the simulation obtained after 100 time steps is shown in **Figure 6b**. The Li distributions obtained for pure a-Si (blue curve) and 5% methylated a-Si (red curve) are plotted as a function of the plane position in the grid, from $z = 1$ (basal plane) to $z = 30$. Noteworthy, the methylated sample and the non-methylated sample exhibit a shape closely similar to the experimental Li^- profile obtained in the ToF-SIMS experiments on partially lithiated methylated amorphous silicon and amorphous silicon, respectively (**Figure 5a**). Close to the basal plane the Li concentration are similar in the two cases. Sharp interfaces are observed in both cases at $z \sim 4$. At z values above 4, the blue curve drops steeply whereas the red curve is decreasing slower as a function of z. Therefore, no Li is observed beyond this interface in pure a-Si but Li is still present in methylated a-Si at a lower concentration than close to the surface. The simulation indicates that deeper is the considered location in the layer, larger is the proportion of lithiated states which are void sites. Therefore, our simulation implements an easier Li transport through nanovoids when going deeper and deeper in the modeled layer. The simulation results make the assumptions plausible: compared with pure a-Si, the distinct shape of the Li^- profile recorded in partially lithiated 5% methylated a-Si could be due to the nano-voids created by the presence of methyl groups.

Finally, the distinction of three concentration ranges in 5% methylated a-Si and only two in a-Si can be reassessed. It could be considered that the Li traces (a-Si) and the sloping profiles (5% methylated a-Si) extending beyond the Li-rich region are the consequence of a similar mechanism of lithiation, more significant in 5% methylated a-Si than in a-Si. To put it another way, it might be considered that nanovoids exist in a-Si even in the absence of methyl groups, but in a lower amount than in 5% methylated a-Si, accounting for the respective intensities of the Li^- intensity in the considered ranges. The existence of nanovoids in pure a-Si is consistent with the results of SAXS investigations.[43] However, it looks that they are not efficiently

contributing to the Li transport in a-Si, as it can be concluded from the lower Li^- intensity. An efficient contribution of nanovoids to the Li transport requires that they form a quasi-percolating network. Percolation is a critical phenomenon, and lowering the concentration of nanovoids significantly below the percolation threshold makes the associated transport mechanism totally inefficient. As a matter of fact, performing simulations with a concentration in nanovoids set to zero or to the value measured by SAXS for a-Si lead to undistinguishable results.[43] Therefore, the identification of a third Li concentration range due to Li transport via nanovoids, present in 5% methylated a-Si but not in a-Si, provides a fully consistent picture.

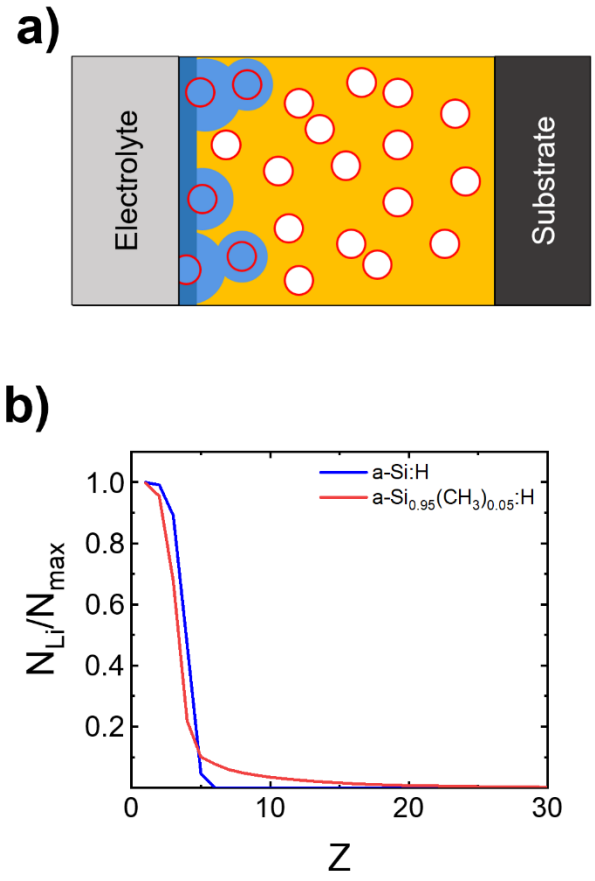

Figure 6. (a) sketch of the model implemented in the simulation; (b) Simulated profiles: Li concentration is plotted as a function of z, from $z = 1$ (basal plane) to $z = 30$ for pure a-Si (in blue) and 5% methylated a-Si sample (in red) after 100-time units.

5. CONCLUSIONS

In conclusion, ToF-SIMS offers a unique opportunity to experimentally determine the lithium depth profile during the first lithiation of thin films. For that purpose, the use of substrates with very flat surfaces, such as silicon wafers, offers a decisive advantage. For silicon-based thin-film electrodes which experience a large swelling during their electrochemical lithiation, the practical depth resolution is not limited by instrumental limits, but by the surface roughening induced by the swelling. In methylated amorphous silicon, the first lithiation of the material takes place according to a biphasic mechanism, like in crystalline or amorphous silicon. In the ToF-SIMS lithium profiles, this process gives rise to the presence of a heavily lithiated region close to the layer surface. Strikingly, in spite of the huge concentration gradient present at the inner side of this region, the lithium profile appears frozen: no lithium motion is recorded on a several hour timescale after the interruption of the lithiation. In addition to this common feature of amorphous silicon and methylated amorphous silicon, a clear difference appears outside the heavily lithiated region, when going deeper in the layer: the lithium concentration significantly drops in pure amorphous silicon (as expected according to a standard biphasic mechanism), whereas a non-null sloping lithium concentration is detected in methylated amorphous silicon. This special profile shape is attributed to the presence of nanovoids which can generate faster paths for in-depth lithium invasion in the material. Therefore, even when electrochemical conditions are chosen in order to obtain an in-plane spatially uniform lithiation of the material, the in-depth lithiation remains non-homogeneous at the atomic scale, due to the generation of easy lithiation paths. To put it in another way, the local rearrangement of the silicon network around methyl groups which generates nanovoids turns to have a long-range impact on lithium transport during the first lithiation of the material. The impact of methyl groups on the first lithiation of the material can also be paralleled with the improved resistance of methylated amorphous silicon to lithiation/delithiation cycles. In

spite of the extended structural changes experienced by the material upon lithiation/delithiation, the ever presence of methyl groups can still be assumed to keep an impact on the local atomic arrangement and Li transport in the material, which might contribute to its increased resistance to electrochemical cycling.

ASSOCIATED CONTENT

Supporting Information

The supporting Information is available free of charge at

Additional information about the home-made cell used for the electrochemical cycling, the influence of the lithiation current on the homogeneity of the first lithiation of (methylated) a-Si, the importance of the lithiation homogeneity on the acquisition of reliable ToF-SIMS profiles, the potential-charge curves of the a-Si and 5% methylated a-Si electrodes during their partial lithiation prior to ToF-SIMS analysis.

AUTHOR INFORMATION

Corresponding Author

François Ozanam – *Laboratoire de Physique de la Matière Condensée, CNRS, Ecole polytechnique, Institut Polytechnique de Paris, 91120 Palaiseau, France;*

- orcid.org/0000-0003-0002-8372; Email: francois.ozanam@polytechnique.edu

Authors

Yue Feng – *Laboratoire de Physique de la Matière Condensée, CNRS, Ecole polytechnique, Institut Polytechnique de Paris, 91120 Palaiseau, France;*

- orcid.org/0000-0002-2134-3980

Bon-Min Koo – *Laboratoire de Physique de la Matière Condensée, CNRS, Ecole polytechnique, Institut Polytechnique de Paris, 91120 Palaiseau, France*

Antoine Seyeux – *PSL Research University, CNRS - Chimie ParisTech, Institut de Recherche de Chimie Paris (IRCP), Physical Chemistry of Surfaces Group, 75005 Paris, France;* • orcid.org/0000-0002-3062-8961

Jolanta Światowska – *PSL Research University, CNRS - Chimie ParisTech, Institut de Recherche de Chimie Paris (IRCP), Physical Chemistry of Surfaces Group, 75005 Paris, France;* • orcid.org/0000-0002-3727-0499

Catherine Henry-de-Villeneuve – *Laboratoire de Physique de la Matière Condensée, CNRS, Ecole polytechnique, Institut Polytechnique de Paris, 91120 Palaiseau, France;* • orcid.org/0000-0002-8668-3070

Michel Rosso – *Laboratoire de Physique de la Matière Condensée, CNRS, Ecole polytechnique, Institut Polytechnique de Paris, 91120 Palaiseau, France;* • orcid.org/0000-0003-0886-1588

Author Contributions

[§]Y.F. and B.-M.K. contributed equally to this work. B.-M.K. and A.S. performed experiments on a-Si, and Y.F. and A.S. performed experiments on methylated a-Si. A.S., J.S., C.H.d.V., M.R. and F.O. defined methodology. Y.F. performed data analysis. M.R. performed modelling. Y.F. and F.O. wrote the original draft of the manuscript on the basis of discussion with all authors. A.S., J.S., C.H.d.V. and M.R. performed extensive review and editing of the manuscript.

Notes

The authors declare no competing financial interest.

ACKNOWLEDGEMENTS

Délégation Générale de l'Armement (DGA) is gratefully acknowledged for financial support. This work was produced within the framework of the Energy4Climate Interdisciplinary Center (E4C) of IP Paris and Ecole des Ponts ParisTech, supported by 3rd Programme d'Investissement d'Avenir (ANR-18-EUR-006-02).

REFERENCES

1. Zuo, X.; Zhu, J.; Müller-Buschbaum, P.; Cheng, Y.-J., Silicon Based Lithium-Ion Battery Anodes: a Chronicle Perspective Review. *Nano Energy* **2017**, 31, 113-143.
2. Green, M.; Fielder, E.; Scrosati, B.; Wachtler, M.; Moreno, J. S., Structured Silicon Anodes for Lithium Battery Applications. *Electrochemical and Solid State Letters* **2003**, 6, A75.
3. Limthongkul, P.; Jang, Y.-I.; Dudney, N. J.; Chiang, Y.-M., Electrochemically-Driven Solid-State Amorphization in Lithium-Silicon Alloys and Implications for Lithium Storage. *Acta Materialia* **2003**, 51, 1103-1113.
4. Nanda, J.; Datta, M. K.; Remillard, J. T.; O'Neill, A.; Kumta, P. N., In situ Raman Microscopy During Discharge of a High Capacity Silicon–Carbon Composite Li-Ion Battery Negative Electrode. *Electrochemistry Communications* **2009**, 11, 235-237.
5. Chae, S.; Choi, S. H.; Kim, N.; Sung, J.; Cho, J., Integration of Graphite and Silicon Anodes for the Commercialization of High-Energy Lithium-Ion Batteries. *Angewandte Chemie International Edition* **2020**, 59, 110-135.
6. Wu, H.; Cui, Y., Designing Nanostructured Si Anodes for High Energy Lithium Ion Batteries. *Nano Today* 2012, 7, 414-429.
7. Zhao, X.; Lehto, V.-P., Challenges and Prospects of Nanosized Silicon Anodes in Lithium-Ion Batteries. *Nanotechnology* **2020**, 32, 042002.
8. Su, X.; Wu, Q.; Li, J.; Xiao, X.; Lott, A.; Lu, W.; Sheldon, B. W.; Wu, J., Silicon-Based Nanomaterials for Lithium-Ion Batteries: A Review. *Advanced Energy Materials* **2014**, 4, 1300882.
9. Ashuri, M.; He, Q.; Shaw, L. L., Silicon as a Potential Anode Material for Li-Ion Batteries: where Size, Geometry and Structure Matter. *Nanoscale* **2016**, 8, 74-103.
10. Wu, F.; Maier, J.; Yu, Y., Guidelines and Trends for Next-Generation Rechargeable Lithium and Lithium-Ion Batteries. *Chemical Society Reviews* **2020**, 49, 1569-1614.
11. Xu, C.; Lindgren, F.; Philippe, B.; Gorgoi, M.; Björefors, F.; Edström, K.; Gustafsson, T., Improved Performance of the Silicon Anode for Li-Ion Batteries : Understanding the Surface Modification Mechanism of Fluoroethylene Carbonate as an Effective Electrolyte Additive. *Chemistry of Materials* **2015**, 27, 2591-2599.
12. Foss, C. E. L.; Müssig, S.; Svensson, A. M.; Vie, P. J. S.; Ulvestad, A.; Mæhlen, J. P.; Koposov, A. Y., Anodes for Li-Ion Batteries Prepared from Microcrystalline Silicon and Enabled by Binder's Chemistry and Pseudo-Self-Healing. *Scientific reports* **2020**, 10, 13193.
13. Shen, B. H.; Veith, G. M.; Tenhaeff, W. E., Silicon Surface Tethered Polymer as Artificial Solid Electrolyte Interface. *Scientific reports* **2018**, 8, 11549.
14. Wu, Z.-Y.; Lu, Y.-Q.; Li, J.-T.; Zanna, S.; Seyeux, A.; Huang, L.; Sun, S.-G.; Marcus, P.; Światowska, J., Influence of Carbonate Solvents on Solid Electrolyte Interphase Composition over Si Electrodes Monitored by In Situ and Ex Situ Spectroscopies. *ACS omega* **2021**, 6, 27335-27350.
15. Obrovac, M. N.; Christensen, L., Structural Changes in Silicon Anodes during Lithium Insertion/Extraction. *Electrochemical and Solid-State Letters* **2004**, 7, A93.
16. McDowell, M. T.; Lee, S. W.; Nix, W. D.; Cui, Y., 25th anniversary article: Understanding the Lithiation of Silicon and Other Alloying Anodes for Lithium-Ion Batteries. *Advanced materials* **2013**, 25, 4966-85.

17. Cao, C.; Steinrück, H.-G.; Shyam, B.; Toney, M. F., The Atomic Scale Electrochemical Lithiation and Delithiation Process of Silicon. *Advanced Materials Interfaces* **2017**, 4, 1700771.
18. Solomon, I.; Schmidt, M. P.; Tran-Quoc, H., Selective Low-Power Plasma Decomposition of Silane-Methane Mixtures for the Preparation of Methylated Amorphous Silicon. *Physical Review B* **1988**, 38, 9895-9901.
19. Touahir, L.; Cheriet, A.; Dalla Corte, D. A.; Chazalviel, J.-N.; Henry de Villeneuve, C.; Ozanam, F.; Solomon, I.; Keffous, A.; Gabouze, N.; Rosso, M., Methylated Silicon: A Longer Cycle-Life Material for Li-Ion Batteries. *Journal of Power Sources* **2013**, 240, 551-557.
20. Koo, B. M.; Corte, D. A. D.; Chazalviel, J.-N.; Maroun, F.; Rosso, M.; Ozanam, F., Lithiation Mechanism of Methylated Amorphous Silicon Unveiled by Operando ATR-FTIR Spectroscopy. *Advanced Energy Materials* **2018**, 8, 1702568.
21. Chon, M. J.; Sethuraman, V. A.; McCormick, A.; Srinivasan, V.; Guduru, P. R., Real-Time Measurement of Stress and Damage Evolution during Initial Lithiation of Crystalline Silicon. *Physical Review Letters* **2011**, 107, 045503.
22. Liu, X. H.; Wang, J. W.; Huang, S.; Fan, F.; Huang, X.; Liu, Y.; Krylyuk, S.; Yoo, J.; Dayeh, S. A.; Davydov, A. V.; Mao, S. X.; Picraux, S. T.; Zhang, S.; Li, J.; Zhu, T.; Huang, J. Y., In Situ Atomic-Scale Imaging of Electrochemical Lithiation in Silicon. *Nature nanotechnology* **2012**, 7, 749-756.
23. McDowell, M. T.; Lee, S. W.; Harris, J. T.; Korgel, B. A.; Wang, C.; Nix, W. D.; Cui, Y., In Situ TEM of Two-Phase Lithiation of Amorphous Silicon Nanospheres. *Nano letters* **2013**, 13, 758-764.
24. Wang, J. W.; He, Y.; Fan, F.; Liu, X. H.; Xia, S.; Liu, Y.; Harris, C. T.; Li, H.; Huang, J. Y.; Mao, S. X.; Zhu, T., Two-Phase Electrochemical Lithiation in Amorphous Silicon. *Nano letters* **2013**, 13, 709-15.
25. Pereira-Nabais, C.; Światowska, J.; Chagnes, A.; Ozanam, F.; Gohier, A.; Tran-Van, P.; Cojocaru, C.-S.; Cassir, M.; Marcus, P., Interphase Chemistry of Si Electrodes Used as Anodes in Li-Ion Batteries. *Applied Surface Science* **2013**, 266, 5-16.
26. Pereira-Nabais, C.; Światowska, J.; Rosso, M.; Ozanam, F.; Seyeux, A.; Gohier, A.; Tran-Van, P.; Cassir, M.; Marcus, P., Effect of Lithiation Potential and Cycling on Chemical and Morphological Evolution of Si Thin Film Electrode Studied by ToF-SIMS. *ACS Applied Materials & Interfaces* **2014**, 6, 13023-13033.
27. Bordes, A.; De Vito, E.; Haon, C.; Secouard, C.; Montani, A.; Marcus, P., Investigation of Lithium Insertion Mechanisms of a Thin-Film Si Electrode by Coupling Time-of-Flight Secondary-Ion Mass Spectrometry, X-ray Photoelectron Spectroscopy, and Focused-Ion-Beam/SEM. *ACS Applied Materials & Interfaces* **2015**, 7, 27853-27862.
28. Feng, Y.; Ngo, T. D. T.; Panagopoulou, M.; Cheriet, A.; Koo, B. M.; Henry-de-Villeneuve, C.; Rosso, M.; Ozanam, F., Lithiation of Pure and Methylated Amorphous silicon: Monitoring by Operando Optical Microscopy and Ex Situ Atomic Force Microscopy. *Electrochimica Acta* **2019**, 302, 249-258.
29. Feng, Y.; Cheriet, A.; Panagopoulou, M.; Aureau, D.; Rowe, A. C.; Henry-de-Villeneuve, C.; Rosso, M.; Ozanam, F., Controlling Homogeneity of the First Lithiation in Methylated Amorphous Silicon. *Electrochimica Acta* **2022**, 403, 139655.
30. Solomon, I.; Schmidt, M. P.; Sénémaud, C.; Driss Khodja, M., Band Structure of Carbonated Amorphous Silicon studied by Optical, Photoelectron, and X-Ray Spectroscopy. *Physical Review B* **1988**, 38, 13263-13270.
31. M. Bhatnagar and I. Solomon, unpublished results.
32. M. Bhatanagar, PhD thesis **1992**, University Paris 6.
33. Lewis, R.; Morabito, J.; Tsai, J., Primary Oxygen Ion Implantation Effects on Depth Profiles by Secondary Ion Emission Mass Spectrometry. *Applied Physics Letters* **1973**, 23, 260-262.
34. Priebe, A.; Utke, I.; Pethö, L.; Michler, J., Application of a Gas-Injection System during the FIB-TOF-SIMS Analysis—Influence of Water Vapor and Fluorine Gas on Secondary Ion Signals and Sputtering Rates. *Analytical Chemistry* **2019**, 91, 11712-11722.
35. Van der Heide, P., *Secondary Ion Mass Spectrometry: an Introduction to Principles and Practices*. John Wiley & Sons: **2014**.
36. Benninghoven, A., Surface analysis by Secondary Ion Mass Spectrometry (SIMS). *Surface Science* **1994**, 299-300, 246-260.

37. Ozanam, F.; Rosso, M., Silicon as Anode Material for Li-Ion Batteries. *Materials Science and Engineering: B* **2016**, 213, 2-11.
38. Gao, F.; Hong, W., Phase-Field Model for the Two-Phase Lithiation of Silicon. *Journal of the Mechanics and Physics of Solids* **2016**, 94, 18-32.
39. Zhang, S., Chemomechanical Modeling of Lithiation-Induced Failure in High-Volume-Change Electrode Materials for Lithium Ion Batteries. *npj Computational Materials* **2017**, 3, 7.
40. Zinner, E., Depth Profiling by Secondary Ion Mass Spectrometry. *Scanning* **1980**, 3, 57-78.
41. Seidlhofer, B.-K.; Jerliu, B.; Trapp, M.; Hüger, E.; Risse, S.; Cubitt, R.; Schmidt, H.; Steitz, R.; Ballauff, M., Lithiation of Crystalline Silicon As Analyzed by Operando Neutron Reflectivity. *ACS Nano* **2016**, 10, 7458-7466.
42. Sakai, Y.; Yae, S.; Matsumura, M.; Nakato, Y.; Tsubomura, H., A New Method of Detecting Pinholes Existing in a-Si:H Films. *Solar Energy Materials* **1988**, 17, 89-94.
43. Williamson, D. L.; Mahan, A. H.; Nelson, B. P.; Crandall, R. S., Microvoids in Amorphous $Si_{1-x}C_x$:H Alloys Studied by Small-Angle X-Ray Scattering. *Applied Physics Letters* **1989**, 55, 783-785.

Graphical Abstract